Journal of Quantitative Spectroscopy & Radiative Transfer 118 (2013) 14–25

Contents lists available at SciVerse ScienceDirect

Journal of Quantitative Spectroscopy & Radiative Transfer

journal homepage: www.elsevier.com/locate/jqsrt

High resolution spectroscopic study of C_2H_4: Re-analysis of the ground state and ν_4, ν_7, ν_{10}, and ν_{12} vibrational bands

O.N. Ulenikov [a,*], O.V. Gromova [a,b], Yu. S. Aslapovskaya [a], V.-M. Horneman [c]

[a] Laboratory of Molecular Spectroscopy, Physics Department, National Research Tomsk State University, Tomsk 634050, Russia
[b] Department of Theoretical and Experimental Physics, Institute of Physics and Technology, National Research Tomsk Polytechnic University,
Tomsk 634050, Russia
[c] Department of Physics, P.O. Box 3000, FIN-90014 University of Oulu, Finland

ARTICLE INFO

Article history:
Received 11 August 2012
Received in revised form
20 November 2012
Accepted 25 November 2012
Available online 18 January 2013

Keywords:
Ethylene
High-resolution spectra
Ground state
Spectroscopic parameters

ABSTRACT

We report here the results of high accurate, $(1-2)\times10^{-4}$ cm^{-1}, ro-vibrational analysis of the ethylene molecule in the region of 640–1535 cm^{-1}. More than 1110, 5060, 4670, and 2900 transitions belonging to the ν_4, ν_7, ν_{10}, and ν_{12} bands were assigned in the experimental spectrum with the maximum values of quantum numbers $J^{max.}/K_a^{max.}$, equal to 36/11, 50/21, 40/17 and 48/17, respectively. Rotational and centrifugal distortion parameters of the ground vibrational state were improved on the basis of assigned transitions and high accurate saturated absorption experimental data known from the literature. The inverse spectroscopic problem was solved for the set of strongly interacting $(\nu_4=1)/(\nu_7=1)/(\nu_{10}=1)/(\nu_{12}=1)$ states. The set of 78 parameters obtained from the fit reproduces values of 3644 initial "experimental" ro-vibrational energy levels (more than 13,740 assigned transitions of the ν_4, ν_7, ν_{10}, and ν_{12} bands) with the *rms*=0.00023 cm^{-1}. In this case, the 197 high accurate saturated absorption transitions are reproduced with the *rms*=18.5 kHz.

1. Introduction

Ethylene is a naturally occurring compound in ambient air that affects atmospheric chemistry and the global climate. Ethylene acts as a hormone in plants and its role in plant biochemistry, physiology, mammals' metabolism, and ecology is the subject of extensive research. Due to its high reactivity toward hydroxyl (OH) radicals, ethylene plays a significant role in troposphere chemistry (see, e.g., [1]) and ozone generation. This contribution to atmospheric chemistry makes ethylene a climate-relevant trace gas and its air concentration, sources and sinks are of interest to atmospheric science. Ethylene is one of the most relevant objects of study in astrophysics (see, e.g., [2,3]) and has been found in the atmospheres of giant planets of the Solar system and their satellites, Refs. [4–9]. Ethylene is also important as a prototype example in the development of our understanding of relating spectra, dynamics, and potential hypersurfaces of many organic molecules. The present analysis is part of the spectroscopic high-resolution study of the ethylene molecule in the region of 600–6000 cm^{-1}. During the analysis we found under consideration our experimental data that we are able to improve the results known in the literature, in particular, with regard to the lowest vibrational states $(\nu_4=1)$, $(\nu_7=1)$, $(\nu_{10}=1)$, and $(\nu_{12}=1)$ which are located around 1000 cm^{-1}. The region around 1000 cm^{-1} is the most extensively studied spectroscopic region of C_2H_4, first of all, because of the presence of the strong bands ν_7 (located near 950 cm^{-1}) and ν_{12} (band center near 1440 cm^{-1}). Very weak ν_{10} band (about 16,500 times weaker than ν_7) with the center near 826 cm^{-1} is also

* Corresponding author. Tel.: +7 9627859656.
E-mail addresses: Ulenikov@mail.ru, Ulenikov@phys.tsu.ru (O.N. Ulenikov).

0022-4073/$ - see front matter © 2013 Elsevier Ltd. All rights reserved.
http://dx.doi.org/10.1016/j.jqsrt.2012.11.032

located in the discussed region. Additionally, transitions belonging to the forbidden by symmetry v_4 band can be seen in the experimental spectrum. The last is caused by the borrowing of intensity from the strong v_7 band because of resonance interaction between the $(v_4=1)$ and $(v_7=1)$ states.

The discussed region was a subject of study in numerous publications (see, e.g., [10–21]). Detailed review of publications can be found in [17,21], on that reason we do not reproduce it here. However, we would like to mark that high accurate millimeterwave, submillimeterwave, or saturation absorption spectra were recorded and analyzed in the most of mentioned studies. As for the high resolution Fourier Transform spectra, spectrum in the region of the bands $v_4/v_7/v_{10}$ was recorded for the last time and presented in Ref. [15] (in all later papers FT data from [15] were used in the fit). As for the v_{12} band, an experimental spectrum in the region 1380–1510 cm^{-1} was recorded and discussed for the last time in Ref. [21]. In this case, in [15] spectra were recorded with the sample pressure of 2 Torr and the absorption path length of 1.13 m. Some different sample pressures (maximum value, 751 Pa) and absorption path lengths (maximum value, 360 cm) were used for recording spectra in Ref. [21]. In our case (see, for more details, Section 2) the $P\times L$ was about 5.5 times larger than in Ref. [15] and about two times larger than the largest $P\times L$ value in Ref. [21]. This circumstance (together with a large number of scans in our experiment up to 1794) allowed us to expect that we are able to record and assign considerably a more number of weak lines in experimental spectra (in particular, with higher values of quantum numbers J and K_a than it was in [15,21]). Moreover, in this case, one can expect that even information about the ground vibrational state may be improved.

Section 2 of the present work describes the experimental conditions of the recorded spectrum. Description of the experimental spectrum and results of assignments of transitions can be found in Section 3. In Section 4 we briefly discuss the Hamiltonian model which was used for fitting the experimental line positions. The problems of re-analysis of the ground vibrational state and determination of spectroscopic parameters of the $(v_4=1)$, $(v_7=1)$, $(v_{10}=1)$, and $(v_{12}=1)$ vibrational states are considered in Sections 5 and 6, respectively. In the last case, the 197 high accurate saturated absorption lines of the v_7 and v_{10} bands (absolute frequency accuracy is between 10 and 60 kHz) from Ref. [17] and 13 absent in [17] high accurate transitions from Ref. [16] (absolute frequency accuracy is $\sim$100 kHz) were used in the fit.

2. Experimental details

The analysis is based on measurements in the wavenumber regions 640–1150 and 1245–1535 cm^{-1}. The measured ranges were optically limited with interference filters. The experimental work was performed in the Infrared Laboratory of Oulu with a Bruker IFS-120 HR Fourier Transform spectrometer. The C_2H_4 sample made for laboratory use by AGA (exact purity unknown) was studied with an absorption spectroscopic method at room temperature in a multipath White cell [22]. Because the band v_{10} is considerably (by a factor of $16{,}500\pm2550$ in accordance with [15]) weaker in comparison with the v_7 band, two spectra (I and II) were recorded with different absorption conditions in the region 640–1150 cm^{-1}. The sample pressure was 0.001 and 0.25 Torr for the spectra I and II, respectively. The absorption path length was 48 m in both cases. Rather long registration time was required in these measurements, 1636 scans in 80.8 h and 1414 scans in 69.8 h were registered in the I and II measurements, respectively. Two different spectra (III and IV) were recorded also in the region 1245–1535 cm^{-1} where the v_{12} band is located. In this case, the absorption path length also was 48 m in both cases. Spectra III and IV were recorded with a sample pressure of 0.1 and 0.78 Torr, respectively. The number of scans was 1794 for both spectra.

The instrument was equipped with a Globar source and a KBr beamsplitter made by Bruker Inc. Infrared radiation was detected with a liquid nitrogen cooled mercury–cadmium–telluride detector. The resolution due to the maximum optical path difference was 0.0014 cm^{-1}. The spectrum was calibrated with peaks of the CO_2 v_2 band ($v_0=667.3799154$ (13) cm^{-1}) [23]. The peak positions were calculated with the optimized center of gravity method discussed in Ref. [24]. The accuracy of a peak position in this method depends on the line width, line shape and signal-to-noise ratio (S/N). In the lower region S/N is worse and the accuracy of a well separated single peak with the absorption of 50% is better than 11×10^{-6} cm^{-1}. In the upper region around 1000 cm^{-1} the accuracy is better than 2.5×10^{-6} cm^{-1}. In addition to these the absolute accuracy depends mainly on the accuracy of the used reference source and the calibration process. Near the calibration source the absolute accuracy is better than 2×10^{-5} cm^{-1} and around 1000 cm^{-1} it is better than 3×10^{-5} cm^{-1}. All these evaluated accuracy values are valid only for well separated peaks. The accuracy of blended peaks is worse.

The calibration was also afterwards checked with the results from the laser study of C_2H_4 [17]. The present peak positions seem to be well compatible with laser reference values in the region 950–1000 cm^{-1}. The mean difference between the reference and present values of 72 good lines is -4.4×10^{-5} cm^{-1}. In the region from 1027 to 1072 cm^{-1} there seem to be more systematic differences, because the mean value of the difference of 30 lines is $+7.5\times10^{-5}$ cm^{-1}.

3. Description of the spectrum and assignment of transitions

The survey spectra in the regions of 640–1150 and 1245–1535 cm^{-1}, where the $v_4/v_7/v_{10}$ and v_{12} bands of the C_2H_4 molecule are located, are shown in Figs. 1 and 2, respectively. In this case, the central part of Fig. 1 (red color) corresponds to the lower pressure spectrum I, and the black color parts correspond to the higher pressure spectrum II. In the central part, near 950 cm^{-1}, one can see the strong Q-branch of the v_7 band. The P- and R-branches are also clearly pronounced. The band v_{10} with the center near 826 cm^{-1} is considerably weaker

(see Section 2) than the ν_7 one. On that reason its R-branch is fully overlapped by the ν_7 band. At the same time, the P-branch of the ν_{10} band is seen very clear in the left "black" part of Fig. 1, which corresponds to the spectrum II recorded with a 250 times higher pressure in comparison with spectrum I. Strong *a*-type Coriolis interaction between the states $(\upsilon_{10}=1)$ and $(\upsilon_7=1)$ which leads to borrowing of intensity from the ν_7 band to the ν_{10} one is an additional reason for the appearance of lines of the weak ν_{10} band in the experimental spectrum. The ν_4 band is forbidden by symmetry. As the consequence, its transitions appear in the experimental spectrum only because of the intensity transfer from the $(\upsilon_7=1)$ band to the $(\upsilon_4=1)$ band caused by the strong *c*-type Coriolis interactions between the state $(\upsilon_4=1)$ and $(\upsilon_7=1)$. For that reason, transitions belonging to the ν_4 band are very weak, as a rule, in comparison with transitions of the ν_7 band, and the ν_4 band is not pronounced in Fig. 1. A small part of the high resolution spectrum in the region of *R*-branch of the ν_7 band is presented in Fig. 3 as an illustration (experimental conditions correspond to the "weak" spectrum I). Transitions assigned to the ν_7 band and to the single line of the ν_{10} band are marked by the dark triangles and empty circle, respectively. Three clearly pronounced sets of *Q*-type transitions of the "forbidden" ν_4 band can be seen also. They are marked by dark circles. Unassigned lines probably belong to ν_7 of $^{12}C^{13}CH_4$ (about 2.2%), to hot bands of ν_7 of C_2H_4 from $(\upsilon_{10}=1)$, $(\upsilon_7=1)$ (both about 1.6%), or from $(\upsilon_4=1)$, $(\upsilon_{12}=1)$ (both less than 0.5%).

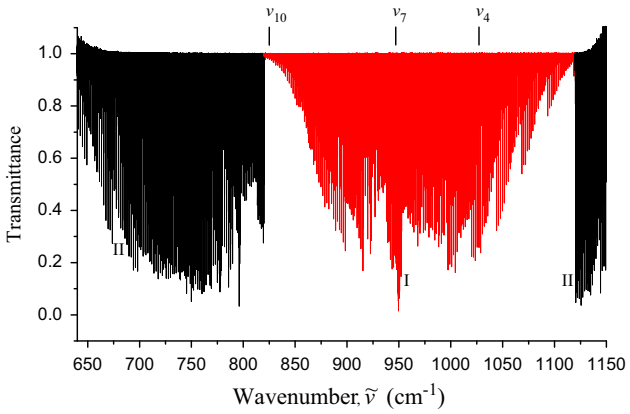

Fig. 1. Survey spectrum of C_2H_4 in the region of 640–1150 cm^{-1}. Two spectra (red "weak", I, and black "strong", II) were recorded with the same absorption path length, L=48 m, but different sample pressure (0.001 Torr for the spectrum I, and 0.25 Torr for the spectrum II). In this case, only wings of the "strong" spectrum II are presented in the figure. (For interpretation of the references to color in this figure legend, the reader is referred to the web version of this article.)

Fig. 2 presents the survey spectrum of the $(\upsilon_{12}=1)$ band. In this case, the weaker spectrum III is shown in the upper part of Fig. 2. The stronger spectrum IV, which allowed us to assigned transitions with high values of quantum number *J*, is presented on the lower part of Fig. 2. Clearly pronounced *P*-, *Q*-, and *R*-branches can be seen in both spectra.

The C_2H_4 molecule is an asymmetric top with the value of the asymmetry parameter $\kappa \simeq (2B-A-C)/(A-C) = -0.915$ and with the symmetry isomorphic to the D_{2h} point symmetry group (see Fig. 4). For convenience of the reader, the symmetry properties in C_2H_4 are shown in Table 1: the list of irreducible representations and table of characters of the D_{2h} symmetry group are presented in columns 1–9; symmetries of rotational operators, J_α, and of direction cosines, $k_{z\alpha}$, are shown in column 10; column 11 allows us to recognize

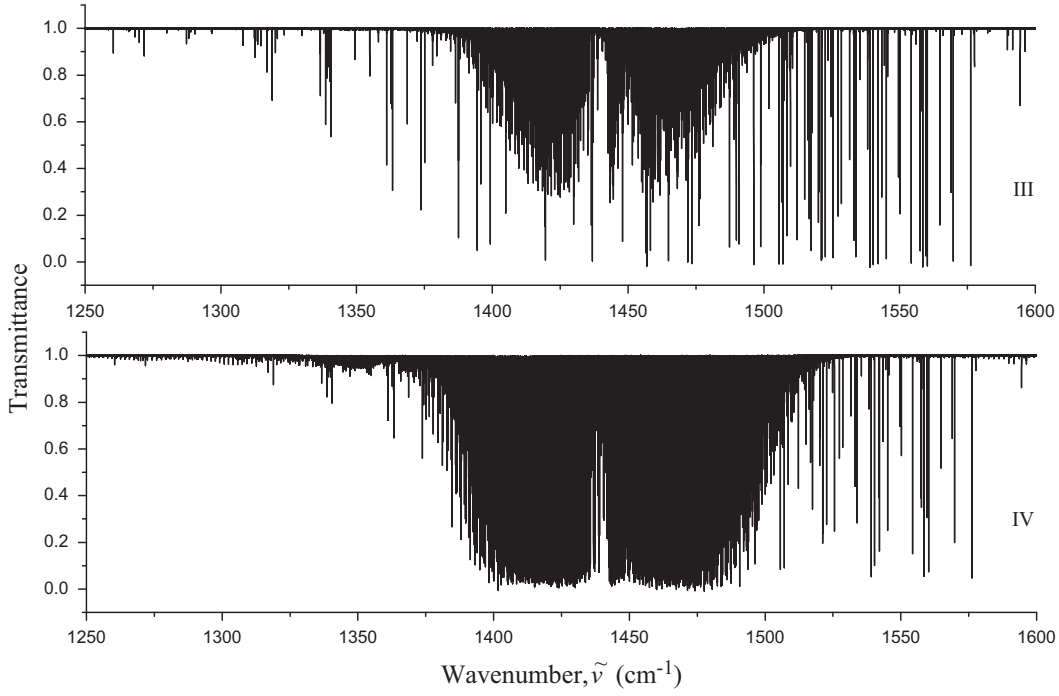

Fig. 2. Survey spectrum of C_2H_4 in the region of 1250–1600 cm^{-1}. Experimental conditions: absorption path length is 48 m for both spectra, III and IV; sample pressure is 0.1 Torr for the spectrum III, and 0.78 Torr for the spectrum IV.

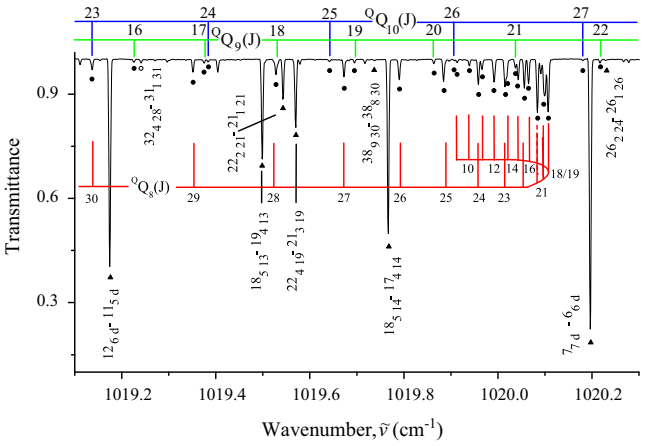

Fig. 3. A small part of the high resolution spectrum of the C_2H_4 molecule in the region of *R*-branch of the ν_7 band. Experimental conditions correspond to the "weak" spectrum I: sample pressure, 0.001 Torr; absorption path length, 48 m; room temperature; 1636 scans. Transitions assigned to the ν_7 band and to the single line of the ν_{10} band are marked by the dark triangles and empty circle, respectively. Three clearly pronounced sets of *Q*-type transitions of the "forbidden" ν_4 band can be seen also. They are marked by dark circles (see text, for more details).

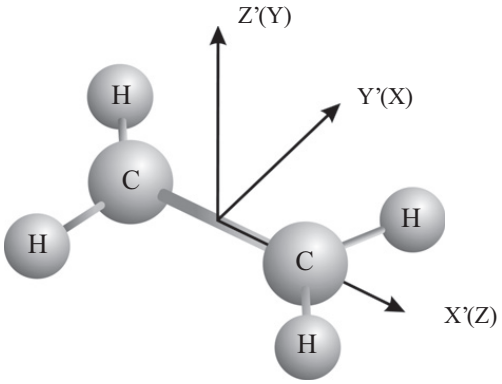

Fig. 4. Axes definitions used in the present work for the ethylene, C_2H_4, molecule. The primed symbols refer to the axis definitions for the D_{2h} symmetry group used in the classification of the vibrational modes. The unprimed symbols refer to the Cartesian axis definitions of the I^r representation of Watson's *A*-reduced effective Hamiltonian.

Table 1
Symmetry types and characters of irreducible representations of the D_{2h} group.

Repr. 1	*E* 2	$\sigma_{x'y'}$ 3	$\sigma_{x'z'}$ 4	$\sigma_{y'z'}$ 5	*i* 6	$C_2(z')$ 7	$C_2(y')$ 8	$C_2(x')$ 9	Rot. 10	Vibr. 11
A_g	1	1	1	1	1	1	1	1		q_1,q_2,q_3
A_u	1	−1	−1	−1	−1	1	1	1		q_4
B_{1g}	1	1	−1	−1	1	1	−1	−1	J_y, k_{zy}	q_5,q_6
B_{1u}	1	−1	1	1	−1	1	−1	−1		q_7
B_{2g}	1	−1	1	−1	1	−1	1	−1	J_x, k_{zx}	q_8
B_{2u}	1	1	−1	1	−1	−1	1	−1		q_9,q_{10}
B_{3g}	1	−1	−1	1	1	−1	−1	1	J_z, k_{zz}	
B_{3u}	1	1	1	−1	−1	−1	−1	1		q_{11},q_{12}

a symmetry of any of 12 vibrational coordinates q_λ of the C_2H_4 molecule. From the analysis of Table 1, it is possible to see that transitions in absorption are allowed only between vibrational states, $(v\Gamma)$ and $(v'\Gamma')$, whose symmetries Γ and Γ' have different indexes "*u*" and "*g*". Moreover, transitions are allowed from the ground vibrational state to the upper vibrational states of the B_{1u}, B_{2u}, or B_{3u} type. Transitions to the upper vibrational state of the A_u-type are forbidden by the symmetry and can appear in the spectrum only because of Fermi or Coriolis type resonance interactions. As can be also seen from column 10, transitions from the ground vibrational state to the vibrational states of the A_g, B_{1g}, B_{2g}, or B_{3g} types are completely forbidden both by the symmetry properties, and because of the absence of interactions between states of the *u* and *g* types. Analysis of Table 1 also shows that

(1) the $B_{1u} \leftarrow A_g$ bands are the *c*-type ones, and the selection rules for them are $\Delta J = 0, \pm 1$ and $\Delta K_a = odd$, $\Delta K_c = even$;
(2) the $B_{2u} \leftarrow A_g$ bands are the *b*-type ones, and the selection rules for them are $\Delta J = 0, \pm 1$ and $\Delta K_a = odd$, $\Delta K_c = odd$;
(3) the $B_{3u} \leftarrow A_g$ bands are the *a*-type ones, and the selection rules for them are $\Delta J = 0, \pm 1$ and $\Delta K_a = even$, $\Delta K_c = odd$.

For this reason the ν_7, ν_{10}, ν_{12}, and ν_4 bands can be identified as the *c*-type, *b*-type, *a*-type, and forbidden one, respectively.

Assignment of transitions was made with the Ground State Combination Differences (GSCD) method. In this case, the rotational energies of the ground vibrational state have been calculated with the parameters from Ref. [17] (for convenience of the reader, ground state parameters from [17] are reproduced in column 3 of Table 2). As the result of assignment, more than 1110, 5060, 4670, and 2900 transitions (in general, more than 13,740 transitions from which 3644 upper rotational energy levels for four upper vibrational states were obtained) with the maximum values of upper quantum numbers, $J^{max.}/K_a^{max.}$, equal to 36/11, 50/21, 40/17 and 48/17 have been assigned to the ν_4, ν_7, ν_{10}, and ν_{12} bands, respectively (for more details, see statistical information in Tables 2 and 3). For comparison, columns 6 and 7 of Table 3 present corresponding analogous information from the before made investigations of discussed bands.

4. Hamiltonian model used for the fit of experimental data

In the present study we used the Hamiltonian in the form (see also [25–28])

$$H^{vib.-rot.} = \sum_{v,\tilde{v}} |v\rangle \langle \tilde{v}| H^{v\tilde{v}}, \quad (1)$$

which takes into account both Fermi-, and any of three Coriolis-type resonance interactions in an asymmetric top molecule. Here the summation extends over all interacting vibrational states. The diagonal operators H_{vv} describe unperturbed rotational structures of the corresponding vibrational states. The nondiagonal operators $H_{v\tilde{v}}$ $(v \neq \tilde{v})$ describe different kinds of resonance interactions between

Table 2
Statistical information for the ν_4, ν_7, ν_{10}, and ν_{12} bands of C_2H_4 molecule (present study).

Band	Center/cm^{-1}	J^{max}	K_a^{max}	N_l[a]	rms_l	m_{l1}[c]	m_{l2}[c]	m_{l3}[c]	N_t[b]	rms_t	m_{t1}[c]	m_{t2}[c]	m_{t3}[c]
1	2	3	4	5	6	7	8	9	10	11	12	13	14
ν_4	1025.58978												
$K_a<14$		36	11	302	2.9	67.3	17.7	15.0	1118	3.0	62.6	21.5	15.9
Total		36	11	302	2.9	67.3	17.7	15.0	1118	3.0	62.6	21.5	15.9
ν_7	948.77090												
$K_a<14$		50	13	1027	1.1	88.2	8.0	3.8	4519	1.2	86.8	8.9	4.3
$K_a\geq 14$		42	21	280	2.4	77.5	13.9	8.6	543	2.5	75.9	13.4	10.7
Total		50	21	1307	1.4	86.7	8.9	4.4	5062	1.5	84.2	11.2	4.6
ν_{10}	825.92676												
$K_a<14$		40	13	804	2.4	63.5	29.1	7.4	4362	2.5	59.9	31.9	8.2
$K_a\geq 14$		35	17	112	5.7	40.4	31.9	27.7	314	5.9	37.6	31.1	31.3
Total		40	17	916	2.7	59.4	28.6	12.0	4676	2.8	56.1	31.7	12.2
ν_{12}	1442.44240												
$K_a<14$		48	13	964	3.0	51.2	29.2	19.6	2632	3.2	49.8	27.8	22.4
$K_a\geq 14$		36	17	122	4.2	30.1	36.8	33.1	270	4.3	28.5	34.9	36.6
Total		48	17	1086	3.2	48.5	30.8	20.7	2902	3.3	45.8	29.3	24.9

[a] N_l is the number of upper levels.
[b] N_t is the number of transitions.
[c] Here $m_i=n_i/N\times 100\%$ (i=1, 2, 3); n_1, n_2, and n_3 are the numbers of levels (transitions) for which the differences $\delta=E^{exp.}-E^{calc.}$ ($\delta=\nu^{exp.}-\nu^{calc.}$) satisfy the conditions $\delta\leq 20\times 10^{-5}$ cm^{-1}, 20×10^{-5} cm$^{-1}<\delta\leq 40\times 10^{-5}$ cm^{-1}, and $\delta>40\times 10^{-5}$ cm^{-1}.

Table 3
Statistical information for the ν_4, ν_7, ν_{10}, and ν_{12} bands of C_2H_4 molecule (overview).

Ref.	Band	Spectrum[a]	Region[b]	Exp. accuracy[c]	$N_t^{(1)}/N_t^{(2)}/N_l$[d]	J^{max}/K_a^{max}	n[e]	$\sigma/rms^{(1)}/rms^{(2)}$[f]
1	2	3	4	5	6	7	8	9
[15]	ν_4	FT+DL	798–1091 (FT+DL)	2–30 (FT) [15]	–/–/105	36/11		
	ν_7	FT+DL+SA	935–1049 (SA)	0.1 (SA) [11]	–/44/403	49/17		
	ν_{10}	FT+DL		10–30 (DL) [15]	–/–/268	39/16		
	Total				–/–/776	49/17	61	0.844/–/–
[17]	ν_4	FT+DL	924–1080 (SA)	0.007–0.02 (SA) [17]	–/–/–	36/11		
	ν_7	FT+DL+SA	798–1091 (FT+DL)	2–30 (FT) [15]	–/195/–	49/17		
	ν_{10}	FT+DL+SA		10–30 (DL) [15]	–/2/–	39/17		
	Total				~5500/197/–	49/17	80	0.825/–/0.015
[20]	ν_4	FT+DL	8–824 GHz (MW)	1–100 kHz (MW) [20]	559/–/–	36/11		
	ν_7	FT+DL+SA+MW	924–1080 (SA)	0.007–0.02 (SA) [17]	3939/208/–	49/17		
	ν_{10}	FT+DL+SA	798–1091 (FT+DL)	2–30 (FT) [15]	980/2/–	39/16		
	Total			10–30 (DL) [15]	~5500/210/–	49/17	78	0.887/–/–
[18]	ν_{12}	FT	1380–1500 (FT)	3 (FT) [18]	1387/–/–	38/15	12	–/3.3/–
[19]	ν_{12}	Jet-cooled FT	700–2400 (FT)	–	963/–/427	33/12	10	–/–/–
[21]	ν_{12}	FT	1380–1510 (FT)	–	1240/–/–	40/–	14	–/1.6/–
This work	ν_4	FT	640–1535 (FT)	1–100 kHz (SA) [20]	1118/–/302	36/11		–/2.9/–
	ν_7	FT+SA	924–1080 (SA)	0.007–0.02 (SA) [17]	5062/208/ 1307	50/21		–/1.4/0.0185
	ν_{10}	FT+SA		2 (FT) (this study)	4676/2/916	40/17		–/2.7/–
	ν_{12}	FT			2902/–/1086	48/17		–/3.2/–
	Total				13,758/210/3644	50/21	78	–/2.3/0.0185

[a] In this column we indicate type of spectra used in the fit: FT, Fourier transform; DL, diode laser; SA, saturation absorption; MW, microwave transitions.
[b] In cm^{-1}.
[c] Experimental accuracy in 10^{-4} cm^{-1}. Reference from which the experimental data are taken is also shown.
[d] The number of transitions and/or levels used in a fit: $N_t^{(1)}$ is the number of FT+DL transitions; $N_t^{(2)}$ is the number of high accurate saturation absorption and/or MW transitions; $N_l^{(1)}$ is the number of levels.
[e] n is the number of fitted parameters.
[f] σ is a unitless standard deviation, see Ref. [31]; the $rms^{(1)}$ is rms of FT+DL data (in 10^{-4} cm^{-1}); the $rms^{(2)}$ is rms of high accurate SA+MW data (in MHz).

the states $|v\rangle$ and $|\tilde{v}\rangle$. The diagonal block operators have the same form for all interacting vibrational states, and they have a form of Watson's Hamiltonian in the A-reduction and I^r representation, Ref. [29]

$$H_{vv}=E^v+[A^v-\tfrac{1}{2}(B^v+C^v)]J_z^2+\tfrac{1}{2}(B^v+C^v)J^2+\tfrac{1}{2}(B^v-C^v)J_{xy}^2$$

$$-\Delta_K^\nu J_z^4-\Delta_{JK}^\nu J_z^2J^2-\Delta_J^\nu J^4-\delta_K^\nu[J_z^2,J_{xy}^2]-2\delta_J^\nu J^2J_{xy}^2$$
$$+H_K^\nu J_z^6+H_{KJ}^\nu J_z^4J^2+H_{JK}^\nu J_z^2J^4+H_J^\nu J^6+[J_{xy}^2,h_K^\nu J_z^4$$
$$+h_{JK}^\nu J^2J_z^2+h_J^\nu J^4]+L_K^\nu J_z^8+L_{KKJ}^\nu J_z^6J^2+L_{JK}^\nu J_z^4J^4$$
$$+L_{KJJ}^\nu J_z^2J^6+L_J^\nu J^8+[J_{xy}^2,l_K^\nu J_z^6+l_{KJ}^\nu J^2J_z^4+l_{JK}^\nu J^4J_z^2+l_J^\nu J^6]+\cdots, \quad (2)$$

where J_α ($\alpha=x,y,z$) are the components of the angular momentum operator defined in the molecule-fixed coordinate system; $J_{xy}^2=J_x^2-J_y^2$; $[\ldots,\ldots]$ denotes anticommutator; A^ν, B^ν, and C^ν are the effective rotational constants connected with the vibrational states (ν), and the other parameters are the different order centrifugal distortion coefficients.

We may distinguish between four types of coupling operators $H^{\nu\tilde\nu}$ ($\nu\neq\tilde\nu$) corresponding to the four different types of resonance interactions which can occur in a set of vibrational states, B_{1u}, B_{2u}, B_{3u}, and A_u, of the D_{2h} asymmetric top molecules. If the product $\Gamma=\Gamma^\nu\otimes\Gamma^{\tilde\nu}$ of the symmetries species of the states ν and $\tilde\nu$ is equal to A_g (i.e., $\Gamma^\nu=\Gamma^{\tilde\nu}$), then the states ν and $\tilde\nu$ are connected by an anharmonic resonance interaction, and the corresponding interaction operator has the form

$$H_{\nu\tilde\nu}={}^{\nu\tilde\nu}F_0+{}^{\nu\tilde\nu}F_{KJ}J_z^2+{}^{\nu\tilde\nu}F_JJ^2+{}^{\nu\tilde\nu}F_{KK}J_z^4+{}^{\nu\tilde\nu}F_{KJ}J_z^2J^2+{}^{\nu\tilde\nu}F_{JJ}J^4+\cdots$$
$$+{}^{\nu\tilde\nu}F_{xy}(J_x^2-J_y^2)+{}^{\nu\tilde\nu}F_{Kxy}[J_z^2,(J_x^2-J_y^2)]+{}^{\nu\tilde\nu}F_{Jxy}J^2(J_x^2-J_y^2)+\cdots. \quad (3)$$

If $\Gamma=B_{1g}$, then the following c-type Coriolis interaction is allowed:

$$H_{\nu\tilde\nu}=iJ_yH_{\nu\tilde\nu}^{(1)}+H_{\nu\tilde\nu}^{(1)}iJ_y+[J_xJ_z]H_{\nu\tilde\nu}^{(2)}+H_{\nu\tilde\nu}^{(2)}[J_xJ_z]$$
$$+[iJ_y,(J_x^2-J_y^2)]H_{\nu\tilde\nu}^{(3)}+H_{\nu\tilde\nu}^{(3)}[iJ_y,(J_x^2-J_y^2)]+\cdots. \quad (4)$$

When $\Gamma=B_{2g}$, a b-type Coriolis interaction of the following type is possible:

$$H_{\nu\tilde\nu}=iJ_xH_{\nu\tilde\nu}^{(1)}+H_{\nu\tilde\nu}^{(1)}iJ_x+[J_yJ_z]H_{\nu\tilde\nu}^{(2)}+H_{\nu\tilde\nu}^{(2)}[J_yJ_z]$$
$$+[iJ_x,(J_x^2-J_y^2)]H_{\nu\tilde\nu}^{(3)}+H_{\nu\tilde\nu}^{(3)}[iJ_x,(J_x^2-J_y^2)]+\cdots. \quad (5)$$

Finally, if the product is $\Gamma=B_{3g}$, then the states ν and $\tilde\nu$ are connected by an a-type Coriolis resonance interaction of the form:

$$H_{\nu\tilde\nu}=iJ_zH_{\nu\tilde\nu}^{(1)}+[J_xJ_y]H_{\nu\tilde\nu}^{(2)}+H_{\nu\tilde\nu}^{(2)}[J_xJ_y]$$
$$+[iJ_z,(J_x^2-J_y^2)]H_{\nu\tilde\nu}^{(3)}+H_{\nu\tilde\nu}^{(3)}[iJ_z,(J_x^2-J_y^2)]+\cdots. \quad (6)$$

The operators $H_{\nu\tilde\nu}^{(i)}$, $i=1,2,3,\ldots$, in Eqs. (4)–(6) have the form:

$$H_{\nu\tilde\nu}^{(i)}=\tfrac{1}{2}{}^{\nu\tilde\nu}C^i+{}^{\nu\tilde\nu}C_K^iJ_z^2+\tfrac{1}{2}{}^{\nu\tilde\nu}C_J^iJ^2+{}^{\nu\tilde\nu}C_{KK}^iJ_z^4+{}^{\nu\tilde\nu}C_{KJ}^iJ_z^2J^2+\tfrac{1}{2}{}^{\nu\tilde\nu}C_{JJ}^iJ^4$$
$$+{}^{\nu\tilde\nu}C_{KKK}^iJ_z^6+{}^{\nu\tilde\nu}C_{KKJ}^iJ_z^4J^2+{}^{\nu\tilde\nu}C_{KJJ}^iJ_z^2J^4+\tfrac{1}{2}{}^{\nu\tilde\nu}C_{JJJ}^iJ^6+\cdots. \quad (7)$$

To prevent confusion in the label notations used, we should mention that we use two sets of axis notation in the C_2H_4 molecule. Firstly, the x-, y- and z-axis are used for labeling of rotational operators J_α ($\alpha=x$, y or z). However, for the point group symmetry assignment of normal modes we use the standard convention in accordance with Ref. [30].

As it can be seen from column 10 of Table 1, four types of vibrational states ($A_g/B_{1g}/B_{2g}/B_{3g}$ only, or $A_u/B_{1u}/B_{2u}/B_{3u}$ only) can be presented in the effective Hamiltonian (1)–(7). It means that there are no interactions between the states of the "g" and "u" types.

5. Re-analysis of the ground vibrational state

As the assignment of transitions in the experimental spectra showed, the rotational structure of the ground vibrational state may be improved. Really, even the best known in the literature Ground State parameters (see, [17,20]) have been obtained on the basis of experimental data from [15]. In this case, FT and diode laser spectra of Ref. [15] have been recorded with worse experimental accuracy than in our case, and transitions with lower values of quantum number K_a have been assigned. As the consequences

(1) ground state combination differences only with $K_a\leq 15$ were used for determination of ground vibrational state parameters and
(2) the set of obtained parameters, which describe very good the rotational energies with $K_a\leq 15$, will be not so good for description of rotational energies with $K_a>15$.

As the illustration of that statement, Fig. 5 presents plots of dependency of differences $\Delta_{J'K_a'K_c'}^{JK_aK_c}={}^{(exp.)}\delta_{J'K_a'K_c'}^{JK_aK_c}-{}^{(calc.)}\delta_{J'K_a'K_c'}^{JK_aK_c}$ (here $\delta_{J'K_a'K_c'}^{JK_aK_c}=E_{JK_aK_c}-E_{J'K_a'K_c'}$) between experimental and calculated values of some sets of ground state combination differences on the value of quantum number J. Curves of different colors (curves I, II, III, and IV) correspond to the values K_a equal 16, 17, 18, and 19, respectively; indexes a and b correspond to two different sets of theoretically calculated

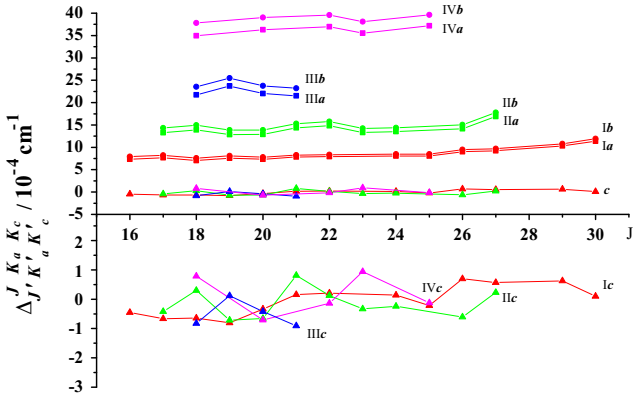

Fig. 5. Plots of dependency of differences $\Delta_{J'K_a'K_c'}^{JK_aK_c}={}^{(exp.)}\delta_{J'K_a'K_c'}^{JK_aK_c}-{}^{(calc.)}\delta_{J'K_a'K_c'}^{JK_aK_c}$ (here $\delta_{J'K_a'K_c'}^{JK_aK_c}=E_{JK_aK_c}-E_{J'K_a'K_c'}$) between experimental and calculated values of some sets of ground state combination differences on the value of quantum number J. Curves of different colors (curves I, II, III, and IV) correspond to the values K_a equal to 16, 17, 18, and 19, respectively. Indexes a and b correspond to two different sets of theoretically calculated combination differences, ${}^{(calc.)}\delta_{J'K_a'K_c'}^{JK_aK_c}$, obtained on the basis of the ground state parameters from Refs. [17,20], respectively. Curves c correspond to the results obtained on the basis of our ground state parameters from column 2 of Table 5. For more details, the same results are reproduced on the bottom part of that figure.

combination differences, ${}^{(calc.)}\delta^{JK_aK_c}_{J'K'_aK'_c}$, obtained on the basis of the ground state parameters from Refs. [17,20], respectively. As one can see from Fig. 5, the values of differences, $\Delta^{JK_aK_c}_{J'K'_aK'_c}$ may achieve the values of 40×10^{-4} cm^{-1}. At the same time, the accuracy of our experiment is about 20 times better. It means that the ground state parameters of both papers [17,20] can be improved.

To make a revision of the ground vibrational state parameters, we constructed 1147 ground state combination differences of the ${}^{(exp.)}\delta^{JK_aK_c}_{J'K'_aK'_c}$-type ($J^{max.}=50$, $K_a^{max.}=19$, $\Delta J=0,\pm1,\pm2$, $\Delta K_a=0,\pm2$) on the basis of transitions assigned to all studied bands in experimental spectra I–IV.[1] Then the constructed ground state combination differences were used as input data in the inverse spectroscopic problem. The saturated absorption transitions from Ref. [17] also gave us possibility to construct 33 very high accurate "experimental" ground state combination differences which are listed in columns 3 and 4 of Table 4. Columns 1 and 2 of that table show the initial saturated absorption transitions which were used in construction of the mentioned "experimental" combination differences. These 33 values also were used as initial data in the inverse spectroscopic problem.

As the result of the weighed fit, we obtained a set of parameters of the ground vibrational state of the C_2H_4 molecule which are presented in column 2 of Table 5 (it should be mentioned that the L_{KKJ}, L_{KJJ}, l_K, etc., centrifugal distortion parameters which are absent in column 2, have been omitted because in the fit procedure their 1σ standard errors were close to the values of obtained parameters, or even more). For comparison, columns 3 and 4 of that table present values of corresponding parameters from earlier studies, Refs. [17,20]. The derived set of parameters reproduces the initial ground state combination differences, obtained from infrared transitions, with the *rms*-deviation of 1.01×10^{-4} cm^{-1} which corresponds to the experimental accuracy of FT data. Column 5 of Table 4 presents differences Δ (in 10^{-6} cm^{-1}) between values of the above-mentioned 33 high accurate "experimental" ground state combination differences and ones theoretically calculated with our parameters from column 2 of Table 5. Analogous results (but from theoretical calculations which were made with the parameters from [17,20], respectively) are shown in column 6. From comparison of data in columns 5 and 6, one can see that our results are better, as a rule. We should mark also that values of parameters obtained in the present study correlate very good with corresponding values known in the literature (see Table 5). At the same time, they give better consent with experimental transitions which correspond to higher (up to $K_a=19$) values of quantum number K_a.

[1] We did not use GS combination differences with $\Delta K_a=\pm4$ which, in principle, could be constructed from a limited number of pairs of assigned transitions. However, at least one transition in any such kind pair is very strong (saturated), or another one is very weak (close to noise). On that reason, corresponding GS combination differences were not used in our analysis.

It would be interesting to estimate a predictive possibility of the obtained set of ground state parameters. To make this, we fulfilled a set of calculations, and results are presented in Fig. 6. At the first calculation we made a list-square fit of all our ground state combination differences with the value $K_a\leq15$. Then the *rms* deviations were determined separately for the sets of states with $K_a=16$, 17, 18, and 19. Results are presented in Fig. 6 (curve I). The curves II, III, and IV illustrate results of analogous calculations of *rms* deviations on the basis of fits of all our combination differences with the value $K_a\leq16$, 17, and 18, respectively. For the last case, an expected interpolation of the *rms* deviation on higher values of quantum number K_a is also shown by dashed line.

6. Ro-vibrational analysis of interacting states ($\nu_4=1$), ($\nu_7=1$), ($\nu_{10}=1$), and ($\nu_{12}=1$)

The new ground state parameters obtained in Section 5 were used then for calculation of ground state rotational energies which, in turn, were used in the re-assignments of transitions in the recorded FT spectra. The list of the more than 13,740 finally assigned transitions is presented in Supplementary Materials. From these transitions we obtained 3644 upper ro-vibrational energies which were used then as input data in a weighted least square fit with the aim to determine rotational, centrifugal distortion, and resonance interaction parameters of the states ($\nu_4=1$), ($\nu_7=1$), ($\nu_{10}=1$), and ($\nu_{12}=1$). Besides 3644 energies obtained from our FT transitions, the 197 high accurate saturated absorption transitions from Ref. [17] and 13 absent in [17] saturated absorption transitions from Ref. [16] were used in the fit procedure as input data. In this case, high accurate transitions from [17] and [16] have been taken with the weights 100 and 5–10, respectively. Upper energy values obtained on the basis of our FTIR experimental data have been taken with the weights 10^{-5} cm$^{-1}/\Delta$ (here Δ is a statistical confidence interval for the upper energy value obtained from some transitions). If the energy of upper state was obtained from the only transitions, it was used with the weight 0.

Results of the fit are presented in columns 3, 5, 7, and 9 of Tables 6 and in 7 (values in parentheses are 1σ statistical confidence intervals). Parameters presented without confidence intervals have been constrained to the values of corresponding parameters of the ground vibrational state (for the convenience of the reader, we re-present in column 2 of Table 6 parameters of the ground vibrational state from column 2 of Table 5). One can see that the values of parameters in columns 3, 5, 7, and 9 correlate very good with the values of corresponding parameters from column 2. Also for comparison, parameters of the states ($\nu_4=1$), ($\nu_7=1$), ($\nu_{10}=1$), and ($\nu_{12}=1$) from Ref. [20] are shown in columns 4, 6, 8, and 10 of Table 6. Again, one can see satisfactory agreement between two sets of parameters. Some small differences can be easily explained by both the differences in parameters of the ground vibrational state (see, columns 2 and 4 of Table 5), and the fact that in our case the number of input data was considerably larger (see, column 6 of Table 3).

The following remark should be made here. In accordance with the general vibration–rotation theory (see, e.g.,

Table 4
High accurate ground state combination differences (GSCD) of C_2H_4 obtained from sub-Doppler experimental data, Ref. [17].

Transition 1	Wavenumber, in cm^{-1} 2	GSCD 3	Value (exp.), in cm^{-1} 4	Δ (calc),[a] in 10^{-6} cm^{-1} 5	Δ (calc),[b] in 10^{-6} cm^{-1} 6
4 0 4←4 1 4	945.5817576	4 1 4–5 1 4	11.2795809	0.5	1.2/1.1
4 0 4←5 1 4	934.3021767				
4 1 3←5 0 5	944.7035103	5 0 5–5 2 3	16.1734814	−0.3	−0.7/−0.8
4 1 3←5 2 3	928.5300289				
5 1 4←4 2 2	947.2863790	4 2 2–5 2 4	9.0470813	−0.2	−0.3/−0.3
5 1 4←5 2 4	938.2392977				
7 3 4←7 2 6	970.0229651	7 2 6–6 4 2	34.6963879	0.1	0.0/−1.0
7 3 4←6 4 2	935.3265772				
7 3 5←6 2 5	982.7606771	6 2 5–6 4 3	47.4535412	0.4	0.5/1.6
7 3 5←6 4 3	935.3071359				
8 3 5 ←7 2 5	983.9970490	7 2 5–8 2 7	13.8727445	0.6	0.0/0.2
8 3 5 ←8 2 7	970.1243045				
7 1 6←6 0 6	968.1127721	6 0 6–6 2 4	16.5317751	−0.5	−0.8/−0.9
7 1 6←6 2 4	951.5809970	6 0 6–7 2 6	28.9005644	−0.6	−1.2/−1.3
7 1 6←7 2 6	939.2122077	6 2 4–7 2 6	12.3687893	−0.1	−0.4/−0.4
7 2 5←6 1 5	972.7448059	6 1 5–7 1 7	8.5076032	0.1	−0.8/−0.6
7 2 5←7 1 7	964.2372027				
9 2 7←9 1 9	966.6256774	9 1 9–10 1 9	26.5495318	0.1	0.9/0.7
9 2 7←10 1 9	940.0761456	10 1 9–9 3 7	9.5366846	−0.1	1.3/1.1
9 2 7←9 3 7	930.5394610	9 1 9–9 3 7	36.0862164	0.1	−0.3/−0.4
10 1 9←9 0 9	976.5128869	9 0 9–10 2 9	35.3897245	0.6	−0.1/−0.3
10 1 9←10 2 9	941.1231624				
10 2 8←9 1 8	977.7494449	9 1 8–10 1 10	9.5632322	−0.1	−1.1/−0.7
10 2 8←10 1 10	968.1862127	9 1 8–11 1 10	39.5602424	0.1	0.6/0.4
10 2 8←11 1 10	938.1892025	10 1 10–11 1 10	29.9970101	0.0	0.7/0.3
11 2 9←11 1 11	970.0061534	11 1 11–11 3 9	38.5042336	−0.3	−1.3/−1.6
11 2 9←11 3 9	931.5019198				
11 3 9←11 2 9	967.2053919	11 2 9–12 2 11	18.2919457	0.0	−1.3/−1.1
11 3 9←12 2 11	948.9134462				
12 2 11←12 1 11	955.0852605	12 1 11–12 3 9	27.5654328	0.2	−0.7/−0.6
12 2 11←12 3 9	927.5198277				
14 11 3[c]←13 10 3	1073.8095319	13 10 3–14 10 4	25.6015243	0.0	0.4/0.5
14 11 4[c]←14 10 4	1048.2080076				
14 2 12←13 1 12	986.1141739	13 1 12– 15 1 14	53.5795312	−0.4	0.4/0.1
14 2 12←15 1 14	932.5346427				
15 3 12←15 2 14	973.8055286	15 2 14–16 2 14	39.3733434	−0.1	0.2/0.5
15 3 12←16 2 14	934.4321852				
15 5 10←15 4 12	987.1903046	15 4 12–14 6 8	50.8763485	1.2	6.0/10.8
15 5 10←14 6 8	936.3139561				
15 4 12←15 3 12	976.4068438	15 3 12–16 3 14	27.5072746	−0.0	−0.5/−0.2
15 4 12←16 3 14	948.8995692				
15 11 4[c]←14 10 4	1075.5812441	14 10 4–15 10 6	27.4319606	0.0	0.6/0.6
15 11 5[c]←15 10 4	1048.1492835				
16 1 15←15 2 13	965.2399820	15 2 13–16 2 15	19.7335200	−0.1	−0.1/ 0.0
16 1 15←16 2 15	945.5064620				
18 7 12←17 6 12	1038.9575382	17 6 12–19 6 14	67.9564936	0.3	−0.8/−0.9
18 7 12←19 6 14	971.0010446				
19 4 15←19 3 17	979.2456597	19 3 17–18 5 13	28.4322967	−0.1	−0.3/−1.6
19 4 15←18 5 13	950.8133630				
24 5 20←23 4 20	1029.8682749	23 4 20–24 4 20	48.5305049	−0.1	−0.8/−0.8
24 5 20←24 4 20	981.3377700	24 4 20–23 6 18	28.9055666	−0.1	−2.0/−3.9
24 5 20←23 6 18	952.4322034	23 4 20–23 6 18	77.4360715	−0.2	1.2/3.1
26 3 23←25 4 21	976.7055364	25 4 21–26 4 23	42.3014327	−0.3	0.7/4.0
26 3 23←26 4 23	934.4041037				

[a] Calculated with our parameters from Table 5.
[b] Calculated with parameters from Table 2 of Refs. [17]/[20].
[c] Two couples of high accurate experimental transitions from Ref. [17], [14 11 3]←[13 10 3]/[14 11 4]←[14 10 4] and [15 11 4]←[14 10 4]/[15 11 5]←[15 10 4], were used in our study because the values of the ground vibrational state rotational energies $E_{[14\ 11\ 3]}/E_{[14\ 11\ 4]}$ and $E_{[15\ 11\ 4]}/E_{[15\ 11\ 5]}$ are the same with accuracy better than 10^{-7} cm^{-1}.

Table 5
Spectroscopic parameters of the ground vibrational state of the C_2H_4 molecule (in cm^{-1}).[a]

Parameter 1	This work 2	From [17][b] 3	From [20][c] 4
A	4.86461997815(72)	4.86462016(4)	4.8646201954(464)
B	1.00105650691(22)	1.00105650(1)	1.0010565039(119)
C	0.82804595595(21)	0.82804599(1)	0.8280459778(117)
$\Delta_K \times 10^4$	0.86470155(39)	0.864798(16)	0.86486844(1953)
$\Delta_{JK} \times 10^4$	0.102336194(71)	0.1023214(36)	0.102319954(3678)
$\Delta_J \times 10^4$	0.014701077(13)	0.01470224(41)	0.014702286(406)
$\delta_K \times 10^4$	0.10153495(38)	0.101590(14)	0.10161652(1391)
$\delta_J \times 10^4$	0.0028179017(46)	0.00281684(15)	0.002816829(149)
$H_K \times 10^8$	0.621279(74)	0.6196(13)	0.624752(1300)
$H_{KJ} \times 10^8$	−0.041497(46)	−0.0424(14)	−0.045941(1185)
$H_{JK} \times 10^8$	0.018693(13)	0.01845(39)	0.0194771(3364)
$H_J \times 10^8$	0.00023588(27)	0.0002501(54)	0.00024347(503)
$h_K \times 10^8$	0.34059(42)	0.346(12)	0.37555(1030)
$h_{JK} \times 10^8$	0.0103566(87)	0.01138(23)	0.0110854(2077)
$h_J \times 10^8$	0.000125178(84)	0.0001098(17)	0.000112776(1669)
$L_K \times 10^{12}$	−0.4467(19)		
$L_{JK} \times 10^{12}$	−0.004492(23)		
$L_J \times 10^{12}$	−0.0000172(28)		

[a] Values in parentheses are 1σ standard errors.
[b] Reproduced from Table 2 of Ref. [17].
[c] Reproduced from Table 2 of Ref. [20].

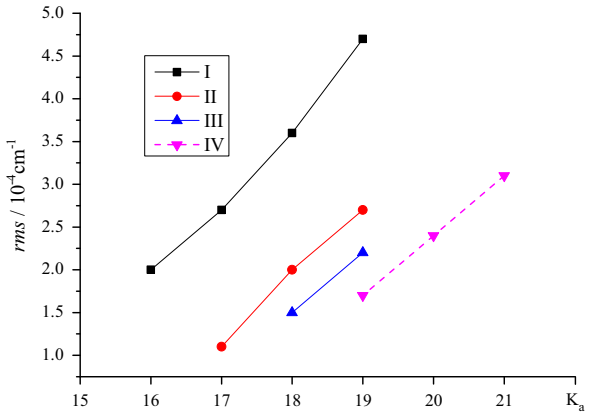

Fig. 6. Illustration of the predictive power of different sets of ground state parameters on the value of quantum number K_a (see text for details).

Ref. [32]), diagonal block's parameters can differ from corresponding parameters of the ground vibrational state no more than for some percent. Following to that statement, we varied only band centers, rotational and the mostly important (Δ_K and Δ_J) centrifugal distortion parameters at the first step of analysis. To achieve a satisfactory correspondence between theoretical and experimental results, the number of varied resonance interaction parameters was larger than usually used in analogous fits. At the second step, we added higher order centrifugal distortion parameters to the fit procedure and reduced the number of resonance interaction parameters. In this case, if a value of varied centrifugal distortion parameter was less or even was comparable with its 1σ statistical confidence interval, such parameter was constrained to the value of corresponding parameter of the ground vibrational state.

The set of parameters obtained from the fit and presented in Tables 6 and 7 reproduces the initial 3644 FT energies with the "*rms*"-deviation equal to 0.00023 cm^{-1} (for more details, see statistical information in Tables 2 and 3). In this case, the 197 initial high accurate saturated absorption transitions from Ref. [17] are reproduced with the *rms*=18.5 kHz. Also, the 13 microwave transitions (experimental accuracy (3–7)$\times 10^{-6}$ cm^{-1}) from Ref. [16], which are absent in [17], are reproduced with the *rms*=5.3$\times 10^{-6}$ cm^{-1}.

As was mentioned in Section 2, near the calibration source the experimental accuracy of lines may be estimated as 2–3$\times 10^{-5}$ cm^{-1}. As the analysis on the basis of the GSCD method shown, it is valid, first of all, for lines of the bands ν_7 and ν_{12} with not very high values of quantum numbers J and K_a in spectra I and III. For weaker lines (lines of the ν_7 and ν_{12} bands with $J+K_a>25-26$; for lines of two other bands; for spectra II and IV), the experimental accuracy is about 2–2.5$\times 10^{-4}$ cm^{-1}. The "*rms*"-deviation of FT data in our fit equal to 0.00023 cm^{-1}, that is close to the mentioned experimental accuracy.

It can be also interesting to compare the results obtained in the present study with the results of analogous studies known in the literature. One can find such detailed comparison in Table 3. In particular, one can see that more than 2.5 times larger number of experimental transitions/energy levels is described by the number of varied parameters which is comparable with the before studies. In this case, it is necessary to take into account that in our fit experimental data for all bands were used.

7. Conclusion

We re-analyzed the high resolution ro-vibrational structures of the ν_4, ν_7, ν_{10}, and ν_{12} bands and assigned

Table 6
Spectroscopic parameters of the ($\nu_4=1$), ($\nu_7=1$), ($\nu_{10}=1$), and ($\nu_{12}=1$) vibrational states of the C_2H_4 molecule (in cm^{-1}).[a]

Parameter 1	Ground state 2	($\nu_4=1$), our work 3	($\nu_4=1$) from [20] 4	($\nu_7=1$), our work 5	($\nu_7=1$) from [20] 6	($\nu_{10}=1$), our work 7	($\nu_{10}=1$) from [20] 8	($\nu_{12}=1$), our work 9	($\nu_{12}=1$) from [20] 10
E		1025.5897759(208)	1025.58928930(12836)	948.77090402(743)	948.77090510(20)	825.9267614(449)	825.92643145(8782)	1442.4424016(216)	1442.443
A	4.86461997815	4.8462200(577)	4.83967600(412)	4.86898055(280)	4.86702423(128255)	4.8734698(277)	4.87528514(128312)	4.85206671(382)	4.8584406
B	1.00105650691	0.99881574(176)	0.99832117(3361)	0.99887651(273)	1.00126775(112)	1.000116099(171)	1.00058469(3324)	1.00392569(812)	1.001479
C	0.82804595595	0.82807345(117)	0.82813460(228)	0.82934142(451)	0.82945984(352)	0.826394802(313)	0.82648000(252)	0.82633727(159)	0.8264808
$\Delta_K\times10^4$	0.86470155	0.86470155	0.786925444(1065278)	0.86470155(796)	1.013649887(1031052)	0.8861073(184)	0.717715382(1372011)	0.866649(126)	0.8647984
$\Delta_{JK}\times10^4$	0.102336194	0.0987461(161)	0.077780725(1121464)	0.1028003(583)	0.098059999(401490)	0.102336194	0.128983612(1074865)	0.1116283(235)	0.10232137
$\Delta_J\times10^4$	0.014701077	0.014701077(938)	0.015524740(6886)	0.01475178(503)	0.014500542(477)	0.014701077	0.013808668(8151)	0.01474409(427)	0.01466900
$\delta_K\times10^4$	0.10153495	0.1017914(862)	0.112413307(856045)	0.09751825(912)	0.095645216(466050)	1.036307(320)	0.075240317(723841)	0.1048415(551)	0.1015900
$\delta_J\times10^4$	0.0028179017	0.0028179017(917)	0.003196895(2688)	0.00280751(269)	0.002669451(248)	0.0028179017	0.002430640(5173)	0.00289684(375)	0.00281683
$H_K\times10^8$	0.621279	0.621279	0.6217815(88430)	0.64669(432)	0.7084123(290859)	0.621279	0.5464641(292050)	0.621279	0.621000
$H_{KJ}\times10^8$	−0.041497	−0.041497	−0.04642090(376770)	−0.041497	−0.03501920(330110)	−0.041497	−0.041350(3411)	−0.041497	−0.0424319
$H_{JK}\times10^8$	0.018693	0.018693	0.0201933(9719)	0.014952(375)	0.0144922(3875)	0.018693	0.0221839(6431)	0.018693	0.0184473
$H_J\times10^8$	0.00023588	0.00023588	0.0002518(87)	0.0002164(331)	0.0001793(48)	0.00023588	0.0002065(185)	0.00023588	0.000245
$h_K\times10^8$	0.34059	0.34059	0.3944995(239239)	0.34059	0.2397887(104210)	0.34059	0.3872099(183440)	0.34059	0.3459264
$h_{JK}\times10^8$	0.0103566	0.0103566	0.0100079(8341)	0.0103566	0.0085999(2312)	0.0103566	0.0098995(6904)	0.0103566	0.0113844
$h_J\times10^8$	0.000125178	0.000125178	0.0000993(95)	0.000125178	0.0000823(18)	0.000125178	0.0001168(95)	0.000125178	0.0001098
$L_K\times10^{12}$	−0.4467	−0.4467		−0.4467		−0.4467		−0.4467	
$L_{JK}\times10^{12}$	−0.004492	−0.004492		−0.004492		−0.004492		−0.004492	
$L_J\times10^{12}$	−0.0000172	−0.0000172		−0.0000172		−0.0000172		−0.0000172	

[a] Values in parentheses are 1σ standard errors.

Table 7
Coriolis interaction parameters for the $(v_4=1,A_u)$, $(v_7=1,B_{1u})$, $(v_{10}=1,B_{2u})$, and $(v_{12}=1,B_{3u})$ vibrational states of the C_2H_4 molecule (in cm^{-1}).

Parameter	Value	Parameter	Value	Parameter	Value
${}^{4,7}C^1_{KK}\times10^7$	−2.7919(317)	${}^{4,7}C^1_{JJ}\times10^9$	0.70268972(989)	${}^{4,7}C^1_{KKJ}\times10^{10}$	0.43483(645)
${}^{4,7}C^2\times10^2$	0.6689444(391)	${}^{4,7}C^2_{J}\times10^5$	−0.017023(856)	${}^{4,7}C^2_{JK}\times10^9$	−0.51473(718)
${}^{4,7}C^2_{JJ}\times10^9$	−0.036952(842)				
$(2B^{x}_{\zeta})^{4,10}$	−1.76868459(642)	${}^{4,10}C^1_{K}\times10^4$	2.83802(302)	${}^{4,10}C^1_{J}\times10^4$	0.0918092(253)
${}^{4,10}C^2\times10^2$	−0.65906(443)	${}^{4,10}C^2_{K}\times10^5$	0.439897(417)	${}^{4,10}C^2_{JK}\times10^9$	−0.32514(181)
${}^{4,10}C^2_{JJ}\times10^9$	−0.07653(748)				
$(2A^{z}_{\zeta})^{4,12}$	−5.5133766(930)	${}^{4,12}C^1_{K}\times10^4$	1.87088(769)	${}^{4,12}C^2_{J}\times10^5$	−0.011565(917)
$(2A^{z}_{\zeta})^{7,10}$	−4.382951799(864)	${}^{7,10}C^1_{K}\times10^4$	1.010374(597)	${}^{7,10}C^1_{KK}\times10^7$	−0.114617(905)
${}^{7,10}C^2\times10^3$	−0.43481(784)	${}^{7,10}C^2_{K}\times10^6$	0.96616(253)	${}^{7,10}C^2_{J}\times10^6$	0.060365(752)
${}^{7,10}C^2_{KK}\times10^9$	−1.2415(673)	${}^{7,10}C^2_{KJ}\times10^9$	−0.192310(742)	${}^{7,10}C^2_{JJ}\times10^9$	−0.0109103(846)
$(2B^{x}_{\zeta})^{7,12}$	−1.34220967(823)	${}^{7,12}C^1_{K}\times10^4$	0.11820(223)	${}^{7,12}C^1_{KKJ}\times10^9$	−0.16043(375)
${}^{7,12}C^2\times10$	−0.1469902(531)	${}^{7,12}C^2_{K}\times10^5$	0.43464(607)	${}^{3,4}C^2_{J}\times10^5$	0.055692(387)
${}^{7,12}C^2_{JJ}\times10^9$	−8.2025(443)	${}^{7,12}C^2_{KKJ}\times10^{11}$	0.6337(286)	${}^{7,12}C^2_{KJJ}\times10^{11}$	−0.053923(768)
$(2C^{y}_{\zeta})^{10,12}$	0.143289(401)	${}^{10,12}C^1_{J}\times10^4$	−0.12482(731)	${}^{10,12}C^1_{KKJ}\times10^{10}$	−3.4082(265)
${}^{10,12}C^1_{KJJ}\times10^{10}$	0.32349(572)	${}^{10,12}C^2\times10^2$	−1.0577(224)	${}^{10,12}C^2_{K}\times10^5$	0.68698(446)
${}^{10,12}C^2_{J}\times10^5$	0.015836(391)	${}^{10,12}C^2_{JJ}\times10^9$	2.1972(856)		

considerably more transitions than was made before. The ground vibrational state was re-analyzed on the basis of our new experimental data. The improved set of ground state parameters was obtained, and used for determination of upper ro-vibrational energy values. The latter were fitted in the Hamiltonian model which takes into account resonance interactions between all four studied vibrational states $(v_4=1)$, $(v_7=1)$, $(v_{10}=1)$, and $(v_{12}=1)$. The obtained parameter from the fit set of 78 parameters reproduces both the initial infrared data, and the high accurate saturated absorption transitions from Refs. [17] and [16] within accuracies close to experimental uncertainties.

Acknowledgments

The work was supported by the FTP "Research and Pedagogical Cadre for Innovative Russia", contract No. 14.B37.21.1298.

Appendix A. Supplementary material

Supplementary data associated with this article can be found in the online version at http://dx.doi.org/10.1016/j.jqsrt.2012.11.032.

References

[1] Abele FB, Heggetad HE. Ethylene: an urban air pollutant. J Air Pollut Control Assoc 1973;23:517–21.
[2] Betz L. Ethylene in IRC+10216. Astrophys J 1981;244:L103–5.
[3] Cernicharo J, Heras AM, Pardo JR, Tielens AGGM, Guelin M, Dartois E, et al. Methylpolyynes and small hydrocarbons in CRL 618. Astrophys J 2001;546:L127–30.
[4] Encrenaz T, Combes M, Zeau Y, Vapillon L, Berenze J. A tentative identification of C_2H_4 in the spectrum of Saturn. Astron Astrophys J 1975;42:355–6.
[5] Hanel RA, Conrath BJ, Flasar FM, Kunde V, Maguire W, Pearl J, et al. Infrared observations of the saturnian system from Voyager 1. Science 1981;212:192–200.
[6] Maguire WC, Hanel RA, Jennings DE, Kunde VG, Samuelson RE. C_3H_8 and C_3H_4 in Titan's atmosphere. Nature 1981;292:683–6.
[7] Kunde VG, Aikin AC, Hanel RA, Jennings DE, Maguire WC, Samuelson RE. C_4H_2, HC_3N and C_2N_2 in Titan's atmosphere. Nature 1981;292:686–8.
[8] Kostiuk T, Espenak F, Mumma MJ, Romani P. Infrared studies of hydrocarbons on Jupiter. Infrared Phys 1989;29:199–204.
[9] Kostiuk T, Romani P, Espenak F, Livengood TA, Goldstein JJ. Temperature and abundances in the jovian auroral stratosphere 2. Ethylene as a probe of the microbar region. J Geophys Res 1993;98:18823–30.
[10] Smith WL, Mills IM. Coriolis perturbation in the infrared spectrum of ethylene. J Chem Phys 1964;40:2095–109.
[11] Herlemont F, Lyszyk M, Lemaire J, Lambeau Ch, Fayt A. Laser spectroscopy of ethylene with waveguide CO_2 and N_2O lasers. J Mol Spectrosc 1979;74:400–8.
[12] Montgomery Jr. GP, Hill JC. High-resolution diode-laser spectroscopy of the 949.2 cm^{-1} band of ethylene. J Opt Soc Am 1975;65:579–85.
[13] Lambeau Ch, Fayt A, Duncan JL, Nakagawa T. The absorption of ethylene in the 10-μm region. J Mol Spectrosc 1980;81:227–47.
[14] Herlemont F, Lyszyk M, Lemaire J, Lambeau Ch, Vleeschouwer M, Fayt A. Saturated absorption of C_2H_4 waveguide laser. J Mol Spectrosc 1982;94:309–15.
[15] Cauuet I, Walrand J, Blanquet G, Valentin A, Henry L, Lambeau Ch, et al. Extension to third-order coriolis terms of the analysis of v_{10}, v_7, and v_4, levels of ethylene on basis of Fourier transform and diode laser spectra. J Mol Spectrosc 1990;139:191–214.
[16] Legrand J, Azizi M, Herlemont F, Fayt A. Saturation spectroscopy of C_2H_4 using a CO_2 laser sideband spectrometer. J Mol Spectrosc 1995;171:13–21.

[17] Rusinek E, Fichoux H, Khelkhal M, Herlemont F, Legrand J, Fayt A. Sub-Doppler study of the v_7 band of C_2H_4 with a CO_2 laser sideband spectrometer. J Mol Spectrosc 1998;189:64–73.
[18] Tan TL, Lau SY, Ong PP, Goh KL, Teo HH. High-resolution Fourier transform infrared spectrum of the v_{12} fundamental band of ethylene (C_2H_4). J Mol Spectrosc 2000;203:310–3.
[19] Hurtmans D, Rizopoulos A, Herman M, Hassan LMS, Perrin A. Vibration–rotation analysis of the jet-cooled v_{12}, v_7+v_8 and v_6+v_{10} absorption bands of C_2H_4. Mol Phys 2001;99:455–61.
[20] Willaert F, Demaison J, Margules L, Mader H, Spahn H, Giesen T, et al. The spectrum of ethylene from microwave to submillimetre-wave. Mol Phys 2006;104:273–92.
[21] Rotger M, Boudon V, Auwera JV. Line positions and intensities in the v_{12} band of ethylene near 1450 cm^{-1}: an experimental and theoretical study. J Quant Spectrosc Radiat Transfer 2008;109: 952–62.
[22] Ahonen T, Alanko S, Horneman VM, Koivusaari M, Paso R, Tolonen AM, et al. A long path cell for the Fourier spectrometer Bruker IFS 120 HR: application to the weak v_1+v_2 and $3v_2$ bands of carbon disulfide. J Mol Spectrosc 1997;181:279–86.
[23] Horneman VM. High accurate peak positions for calibration purposes with the lowest fundamental bands v_2 of N_2O and CO_2. J Mol Spectrosc 2007;241:45–50.
[24] Horneman VM. Instrumental and calculation methods for Fourier transform infrared spectroscopy and accurate standard spectra. Thesis Acta Univ Oul A 1992;239:127.
[25] Ulenikov ON, Tolchenov RN, Koivusaari M, Alanko S, Anttila R. High-resolution Fourier transform spectrum of CH_2D_2: Pentade of the lowest interacting vibrational bands v_4, v_7, v_9, v_5, and v_3. J Mol Spectrosc 1994;167:109–30.
[26] Ulenikov ON, Bekhtereva ES, Grebneva SV, Hollenstein H, Quack M. High resolution Fourier transform spectrum of CH_2D_2 in the region of 2350–2650 cm^{-1}: the bands v_5+v_7, $2v_9$, v_3+v_4, v_3+v_7, and v_5+v_9. Phys Chem Chem Phys 2005;7:1142–51.
[27] Ulenikov ON, Bekhtereva ES, Albert S, Bauerecker S, Hollenstein H, Quack M. High resolution near infrared spectroscopy and vibrational dynamics of dideuteromethane (CH_2D_2). J Phys Chem A 2009;113:2218–34.
[28] Ulenikov ON, Onopenko GA, Bekhtereva ES, Petrova TM, Solodov AM, Solodov AA. High resolution study of the v_5+v_{12} band of C_2H_4. Mol Phys 2010;108:637–47.
[29] Watson JKG. Determination of centrifugal distortion coefficients of asymmetric-top molecules. J Chem Phys 1967;46:1935–49.
[30] Herzberg G. 1st ed.Molecular spectra and molecular structure, infrared and raman spectra of polyatomic molecules, vol. 2. New York: van Nostrand; 1945.
[31] Albritton DL, Schmeltekopf AL, Zare RN. In: Rao KN, editor. Molecular spectroscopy, modern research, II (Chapter 1). New York: Academic Press; 1976.
[32] Papousek D, Aliev MR. Molecular vibrational–rotational spectra.Amsterdam: Elsevier; 1982.